

Design and Control of a Quasi-Direct Drive Soft Hybrid Knee Exoskeleton for Injury Prevention during Squatting

Shuangyue Yu*, Tzu-Hao Huang*, Dianpeng Wang, Brian Lynn, Dina Sayd, Viktor Silivanov, Young Soo Park, Yingli Tian, Fellow, *IEEE*, and Hao Su†, Member, *IEEE*

Abstract—This paper presents a new design approach of wearable robots that tackle the three barriers to mainstay practical use of exoskeletons, namely discomfort, weight of the device, and symbiotic control of the exoskeleton-human co-robot system. The hybrid exoskeleton approach, demonstrated in a soft knee industrial exoskeleton case, mitigates the discomfort of wearers as it aims to avoid the drawbacks of rigid exoskeletons and textile-based soft exosuits. Quasi-direct drive actuation using high-torque density motors minimizes the weight of the device and presents high backdrivability that does not restrict natural movement. We derive a biomechanics model that is generic to both squat and stoop lifting motion. The control algorithm symbiotically detects posture using compact inertial measurement unit (IMU) sensors to generate an assistive profile that is proportional to the biological torque generated from our model. Experimental results demonstrate that the robot exhibits 1.5 Nm torque when it is unpowered and 0.5 Nm torque with zero-torque tracking control. The efficacy of injury prevention is demonstrated with one healthy subject. Root mean square (RMS) error of torque tracking is less than 0.29 Nm (1.21% of 24 Nm peak torque) for 50% assistance of biological torque. Comparing to the squat without exoskeleton, the maximum amplitude of the knee extensor muscle activity (rectus femoris) measured by Electromyography (EMG) sensors is reduced by 30% with 50% assistance of biological torque.

I. INTRODUCTION

Musculoskeletal disorders (MSDs) are a leading cause of injury among various individuals, ranging from workers and soldiers to caregivers, who are exposed to physical workloads [1]. Wearable robots present an attractive solution to mitigate the incidence of injury and augment human performance [2]. Besides recent breakthroughs of wearable robotics in human

augmentation that enhance the human economy and endurance [3-5] and in gait restoration that enhances mobility [6-9], the industrial exoskeleton is an emerging area that presents new opportunities and challenges. Passive [10, 11] and powered exoskeletons [12, 13] have demonstrated effectiveness for injury prevention of upper body and back support. Recently, there is a growing interest in wearable robots for knee joint assistance as cumulative knee disorders account for 65% of lower extremity musculoskeletal disorders [14]. Squatting and kneeling are two of the primary risk factors that contribute to knee disorders [14].

Industrial exoskeletons for knee assistance present new challenges as the required range of motion and the torque assistance are typically much greater than walking. Most of the existing knee exoskeletons are designed for walking assistance [15, 16] and they typically do not allow squat motion due to the interference between the robot and human bodies (e.g. [17, 18]). Like all wearable robots, knee exoskeletons can be generally classified as rigid or soft in terms of actuation and transmission. Quasi-passive knee design was studied in [19] as prosthesis and [20] as exoskeletons. [21] used the series elastic actuator (SEA) to decouple motor inertia and reduce passive output impedance. Keeogo exoskeleton [22] uses high ratio harmonic drive gear to amplify torque of a brushless direct current (BLDC) motor. Soft exoskeletons either using pneumatics [23] or cable transmission [24] represent a trend in wearable robot design.

Discomfort, weight of device and symbiotic control of exoskeleton-human co-robot system to enable fluid movement are considered three key barriers to mainstay practical use of exoskeletons [2, 25]. This paper presents three solutions to tackle those challenges, namely hybrid exoskeleton design approach, quasi-direct drive actuation paradigm, and biomechanics-model based control. Those methods are

This work is supported by the National Science Foundation grant NRI 1830613 and Grove School of Engineering, The City University of New York, City College. Any opinions, findings, and conclusions or recommendations expressed in this material are those of the author (s) and do not necessarily reflect the views of the funding organizations

Shuangyue Yu, Tzu-Hao Huang, Dianpeng Wang, Brian Lynn, Dina Sayd, Viktor Silivanov, and Hao Su are with the Lab of Biomechatronics and Intelligent Robotics, Department of Mechanical Engineering, The City University of New York, City College, New York, NY, 10023, US.

Young Soo Park is with the Applied Materials Division, Argonne National Laboratory, Lemont, IL, 60439, US.

Yingli Tian is with the Department of Electrical Engineering, The City University of New York, City College, New York, NY, 10023, US.

*These authors contributed equally to this work. †Corresponding author. Email: hao.su@ccny.cuny.edu

generic for the design and control of high-performance wearable robots, and industrial knee exoskeleton is instantiated as one example in this work as shown in Fig. 1. The contribution of this work includes 1) a hybrid exoskeleton design that avoids the drawbacks of rigid exoskeletons (heavy and bulky) and textile-based soft exosuits (small moment arm and high-pressure concentration) [26]; 2) a quasi-direct drive actuation paradigm that optimizes comfort to make the robot lightweight and highly-backdrivable (low impedance); 3) a cable-drive mechanism that uses one motor to control both flexion and extension, thus it could reduce weight of the device; 4) a biomechanics model that is generic for both squat and stoop lifting and a control strategy that mitigates musculoskeletal injuries demonstrated with reduced muscle activities.

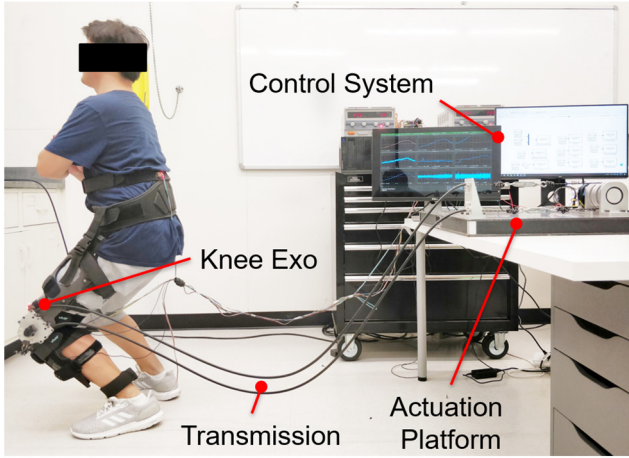


Fig. 1. A healthy subject performs squatting with the unilateral soft knee exoskeleton that uses quasi-direct drive actuation paradigm that consists of high torque density motors and low transmission ratio gears. Bidirectional cable-actuation produces flexion and extension torque with a single motor (less mass).

II. DESIGN REQUIREMENTS

The soft knee exoskeleton is a versatile assistive device designed to augment different knee movements including lifting (both squat and stoop) and walking, though the focus of this paper is squat assistance. Since the focus of this work is to understand feasibility of the design principles and effectiveness of control strategies, the prototype is a tethered design with offboard actuation and its design outcome is transferable to portable exoskeleton design. The design requirement is based on data from healthy human subjects with 80 kg weight and a height of 180 cm without carrying any load [27]. Knee joint assistance during squatting necessitates a broad range of motion (0-130° degrees flexion) and biological joint moment (up to 60 Nm). The torque generated from the robot needs to be delivered at an angular velocity of no less than 2.4 rad/s to effectively synchronize with the user. Though the robot is designed to deliver 72 Nm torque, our control philosophy aims to use small to medium torque by optimizing timing, magnitude, and profile of torque trajectories [3].

TABLE I. DESIGN PARAMETERS OF KNEE EXO FOR DEEP SQUAT

Parameters	Walking	Squat	Our Robot
Range of motion (deg)	10-60	0-130	0-130

Max knee joint moment (Nm)	40	60	72
Max knee joint speed (rad/s)	4.3	2.4	4.4
Exoskeleton moment arm (m)	0.35	0.35	0.35
Actuator min speed (m/s)	0.22	0.12	0.22
Actuator max force (N)	320	480	1250

III. HYBRID EXOSKELETON DESIGN AND QUASI-DIRECT DRIVE ACTUATION USING HIGH TORQUE DENSITY MOTORS

The soft exoskeleton design approach proposed in this paper is hybrid in the sense that it uses cable transmission (like textile-based soft exosuit) while maintains large moment arm (like rigid exoskeletons, thus it requires less force for the same amount of delivered torque by the robot) as shown in Fig. 2. It presents one solution to reduce forces applied to limbs (because of its larger moment arm comparing with textile-based soft exosuits) and pressure concentration (3D scanning and 3D printing based orthotic brace with foam padding are conformable and conformal). Quasi-direct drive actuation [28] [29] using high torque density motors can potentially be designed to be not only more lightweight but also highly-backdrivable and unobtrusive to human movement.

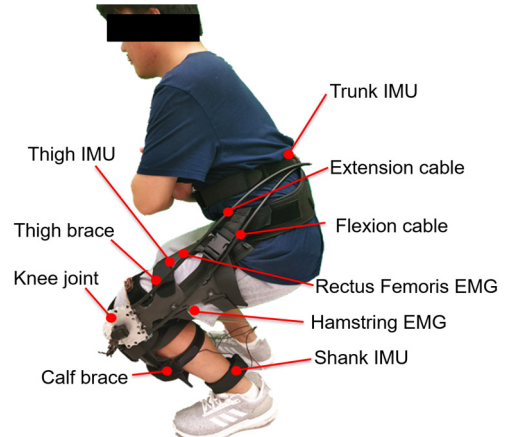


Fig. 2. The knee exoskeleton represents our hybrid design approach in that uses cable transmission (like textile-based soft exosuit) while maintains large moment arm (like rigid exoskeleton). It uses IMU sensors to measure the subject's trunk, thigh, and shank postures to generate hip and knee angles for bio-inspired squat assistance control. Two EMG sensors monitor muscle activities of rectus femoris and hamstring to evaluate the assistance performance of the system.

To enable quasi-direct drive actuation paradigm, it is crucial to design high torque density motors. Our custom designed BLDC motors optimize the mechanical structure, topology, and electromagnetic properties [30, 31]. It uses high-temperature resistive magnetic materials and adopts an outer rotor, flat and concentrated winding structure. Unlike conventional BLDC motors that place windings around rotors, our rotor consists of only the permanent magnet and rotor cover while the winding is attached to stators. This design significantly reduces the inertia and mechanical impedance of the motor while increasing its control bandwidth. Fig. 3 shows the continuous torque density versus air gap radius distribution of our motor and commercial ones [29]. The continuous torque of our motor is 2 Nm and its mass is 274 g. Maxon EC Flat 90 has 0.5 Nm continuous torque with 648 g mass. In the 35-40 mm air gap radius domain, the continuous torque density of

our motor is 7.3 Nm/Kg while T-motor U8 is 3.5 Nm/Kg, and Maxon EC Flat 90 is 1.5 Nm/Kg.

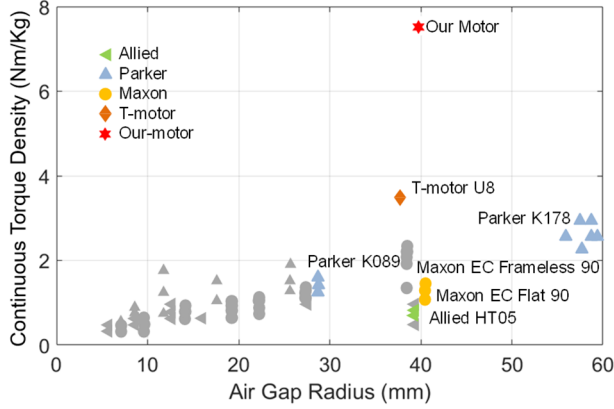


Fig. 3. Continuous torque density versus air gap radius distribution of our motor and other commercial ones.

The quasi-direct drive actuation paradigm was implemented with a tethered actuation platform shown in Fig. 4 (a) as a side view and (b) as a top view. With custom designed 2-stage planetary gears with 36:1 ratio and 172 g, the actuator generates 72 Nm continuous torque and 4.36 rad/s angular velocity. Even though it is a tethered system, the platform is viable to be converted into a portable design as the overall mass of the actuator is only around 500 Kg.

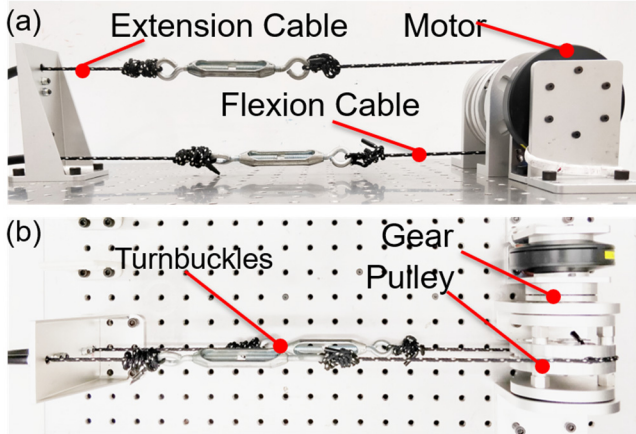


Fig. 4. Side and top view of the quasi-direct drive actuation platform consisting of high torque density motors (custom designed motor that has about 5 times torque density than Maxon brushless DC motors) and low transmission ratio gears (36:1 custom designed planetary gear).

IV. ELECTROMECHANICAL DESIGN

The detailed implementation of the hybrid exoskeleton design approach and the quasi-direct drive actuation principle features a bidirectional cable drive transmission, low-profile knee joint mechanism, and Controller Area Network (CAN) based communication and control electronics for IMU posture sensing and motor control.

A. Bidirectional-Drive Cable Transmission

Our innovative design uses one motor to remotely drive the wearable structure to control both flexion and extension

motion. This mechanism has two advantages. First, it reduces the mass and cost of actuators as conventional cable drive actuation typically uses one motor to control unidirectional motion (flexion or extension) as the cable can only be pulled [32]. Thus, the mass of the actuators in conventional design is roughly doubled as it requires two motors to control bidirectional motion. Second, this allows the placement of system mass in the proximity of the center of mass of the wears to minimize distal mass and energy expenditure caused by mass of a robot.

In our design, actuation is transmitted to the wearable structure through cable and proximal/distal pulley pair. With adequate tensioning the cable will act as a linear spring. In order to obtain high-performance torque control, it is necessary to have adequate pretension for a cable-driven system. The proximal end of the cable drive mechanism has turnbuckles to adjust cable tensions.

B. Low Profile and Lightweight Knee Joint Mechanism

The design consideration of knee joint mechanism is to avoid interference with the human body during squat motion while achieving minimal mass. The knee joint shown in Fig. 5 is the distal portion of the bidirectional cable-drive. The design contains one flexion cable and one extension cable that pass through the distal pulley and terminate at the cable locking mechanism. The load cell connects the thigh and calf braces and plays a key role in force transmission between the cable and the shank plate. The top portion of the knee mechanism is attached to the 3D printed thigh brace while the shank plate is fixed to the calf brace. The terminated cable on the locking mechanism actuates the pulley, thus driving the shank plate via load cell.

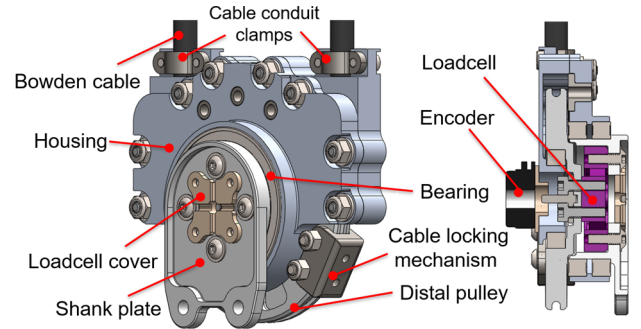


Fig. 5. A section view (left) and an isometric view (right) of the cable-driven knee mechanism that actuates both knee flexion and extension. It is composed of two cable conduit clamps, a distal pulley, a housing to enclose internal components, a load cell cover, an shank plate, a cable locking mechanism (it also prevents knee hyperextension), a ball bearing, an encoder, and a custom load cell that measures up to 50 Nm torque.

The output torque is instrumented by a custom load cell made of 6061 aluminum alloy. In order to assure the work requirements, the load cell is designed and prototyped via finite element analysis (FEA). The outer ring was configured to be fixed and an external torque of magnitude 50 Nm was applied to the inner ring. As shown in Fig. 6, the results of the FE analysis depict that the maximum shear stress, strain, and displacement occur around the middle region of the inner ring. When the external torque of 50 Nm was applied to the inner ring, the maximum shear stress was 369.5 N/mm² (MPa), the maximum strain was 0.01148, and the maximum displacement

was 0.1040 mm. The yield strength of 6061 aluminum alloy is much greater than the calculated stress of the torque sensor. Thus, our load cell meets the strength requirements to be reliably used in our knee exoskeleton.

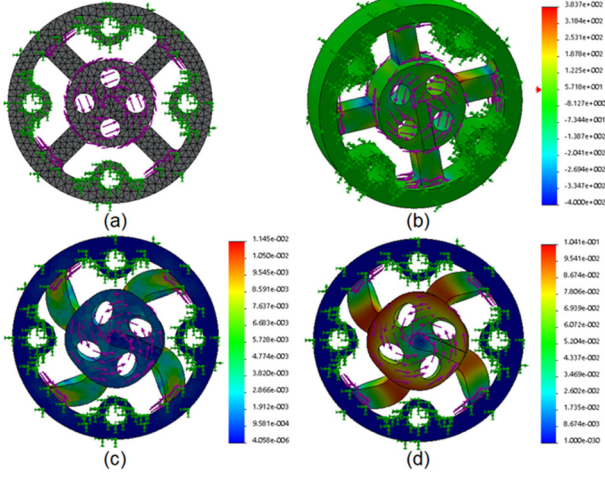


Fig. 6. FEA analysis of flexure joint of the custom designed load cell with 50 Nm range. (a) Mesh grid; (b) Shear stress distribution (MPa); (c) Strain distribution; (d) Displacement (mm).

Furthermore, the exoskeleton is attached to the body via 3D carbon fiber printed braces designed to conform to the human leg. These braces transmit the torque at the pulley knee joint into a pressure distributed along the length of the thigh and shank. Therefore, the appropriate size of wearable arms plays a crucial role in the performance and comfort of the subject wearing the exoskeleton. Three-dimensional infrared scans (Sense 2, MatterHackers Inc.) are taken of the patient's leg and then processed into a three-dimensional CAD model, which are 3D printed using fused deposition modeling (Replicator+, Makerbot Inc.). This model is then reinforced with a carbon fiber and resin composite. The arms are padded in locations of leg contact to aid in comfort. Velcro straps are then wrapped around the leg of the user and are anchored to the exoskeleton arms, thus allowing the exoskeleton to be adjusted for optimal user comfort. Additionally, a large belt wrapped around the user's waist has been designed to adjust to the user's measurements. It is padded and wide enough to distribute the knee weight comfortably.

C. Electronics and Communication

The electronics system has a two-layer configuration architecture: real time target computer as a high-level controller and local motor controller as a low-level controller. The high-level controller consists of two Dell desktops computers. The host computer (Precision Tower 3420, Dell Computer Corp.) compiles and deploys the control algorithm to the target computer (Optiplex 960, Dell Computer Corp.) which runs Matlab Simulink Real-Time (Mathworks Inc.) and executes the real-time control algorithm. The target PC is equipped with a PCI CAN interface card (CAN-AC2-PCI, Softing Industrial Automation GmbH) which sends control commands to the low-level control system in real time and a PCI-e I/O card (ADC, PCIe-6259, National Instrument, Inc.) which acquires sensor signals. An encoder (HEDM-5500#B06, AVAGO Technologies, Inc.), two active EMG electrodes with

330 proportional gain (B&L Engineering), and a custom designed load cell signal can be directly measured by target computer through PCI-e I/O card. The IMUs stream Euler angles to an Arduino Due board by serial ports and the fourth serial port of Arduino Due is used to send the IMU data to the target computer shown in Fig. 5. The low-level controller has a motor driver and a microcontroller (DSP TMS320F28335, Texas Instrument, Inc.) to measure motor status (i.e. current, velocity, and position), communicate with the target computer through CAN bus.

V. SQUAT ASSISTIVE CONTROL STRATEGIES

We derive a biomechanics model that is generic for both squat and stoop lifting and propose the control strategy that explicitly generates the knee torque trajectory with thigh and knee joint angle measurement using IMU sensors. [33] proposed assistive algorithms for a squat exoskeleton. But the model assumed that the back posture of the subject was straight and the trunk angle was zero. It only used knee joint to calculate the torque reference and is lack of the posture information of the hip and trunk. However, during lifting (squat and stoop) the back angle varies and it significantly affects the knee joint torque. The assistive strategy is shown in Fig. 7 is composed of high-level torque control and low-level motor control. The three IMUs detect the hip and knee joint angles in the global coordination. The human dynamic model is used to calculate the human knee torque during squatting.

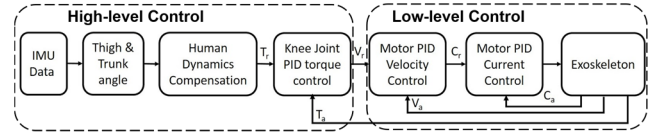


Fig. 7. The diagram of the bio-inspired squat assistance control algorithm. The high-level controller generates a reference torque profile using our generic lifting biomechanics model to compensate for human dynamics. The τ_r and τ_a are the torque reference and actual measured torque; the V_r and V_a are the velocity reference and actual estimated velocity; the C_r and C_a are the current reference and actual measured current.

A. Human Quasi-Static Model during Squat

In this study, a human biomechanics model shown in Fig. 8 is derived to calculate the biological knee joint torque and assistive torque. This model is customizable to different individuals in the sense that the calculated torque can be adjusted according to the subject's weight and height through the weight ratio (subject weight M_{sb} /human model weight M_w) and height ratio (subject height L_{sb} /human model height L_H). Because squatting is relatively slow, the joint torque could be derived with a quasi-static motion and the inertia term is neglected in this study. The knee joint torque (τ_k) in the quasi-static model can be derived from equation (1). Here the knee extension is defined as the positive direction for the knee joint torque τ_k and reference torque τ_r . The clockwise direction is defined as the positive direction for the trunk angle θ_b , the thigh angle θ_t , and the shank angle θ_s . M_t is the mass of the head, neck, thorax, abdomen, pelvis, arms, forearms, and hands, and M_l is the mass of thigh, L_b is the length between the center of mass of M_b and the hip pivot, whereas L_t is the length of thigh between the hip pivot and knee pivot, L_{lc} is the

length between the center of mass of M_t and the knee pivot, g is the gravitational constant, θ_b is the trunk angle and θ_t is the thigh angle.

$$\tau_k = -0.5 \cdot [M_b \cdot g \cdot (L_b \cdot \sin\theta_b + L_t \cdot \sin\theta_t) + M_t \cdot g \cdot L_{tc} \cdot \sin\theta_t] \quad (1)$$

The desired assistive torque of the exoskeleton (τ_r) was defined as equation (2) in our proposed assistive control.

$$\tau_r = \alpha \cdot \tau_k \quad (2)$$

As long as the gain α is positive, the exoskeleton will assist the human. It can be used to reduce the loading and increase the endurance for workers. On the other hand, when the gain α is negative, the exoskeleton will resist the human. It can be used to increase the muscle strength for health human in fitness or patient with movement impairment in rehabilitation.



Fig. 8. The annotations for the mass of head, neck, thorax, abdomen, pelvis, arms, forearms, and hands (M_b), the mass of thigh (M_t), the length between the center of mass of M_t and the hip pivot (L_b), the length of thigh (M_t), the length between the hip pivot and knee pivot (L_t), the length between the center of mass of M_t and the knee pivot (L_{tc}), the trunk angle (θ_b), the thigh angle (θ_t), and the shank angle (θ_s).

Based on the (3)-(7) equations, the parameters L_b , L_t , L_{tc} , M_b , M_t are calculated by data in Table II obtained from the anthropometry research [34]. This model is customizable because each individual's weight and height can be normalized by M_W and L_H respectively. M_{sb} is the mass of the subject and the L_{sb} is the height of the subject. M_W is the total mass of the human model and L_H is the total height of the human model from the anthropometry study.

$$M_b = (M_{sb}/M_W) \cdot \sum_{i=1}^8 M_i \quad (3)$$

$$M_t = (M_{sb}/M_W) \cdot M_9 \quad (4)$$

$$L_b = (L_{sb}/L_H) \cdot \{[\sum_{i=1}^8 (M_i \cdot L_i) / \sum_{i=1}^8 (M_i)] - L_{12}\} \quad (5)$$

$$L_t = (L_{sb}/L_H) \cdot (L_{12} - L_{13}) \quad (6)$$

$$L_{tc} = (L_{sb}/L_H) \cdot (L_9 - L_{13}) \quad (7)$$

TABLE II. THE HUMAN SEGMENT PARAMETERS

#	Segment	M_i : Mass (Kg) Total Weight M_W : 81.4 Kg	L_i : Length between Center of Mass to Ground (m) Total Height L_H : 1.784 m
1	Head	M_1 : 4.2 Kg	L_1 : 1.679 m
2	Neck	M_2 : 1.1 Kg	L_2 : 1.545 m
3	Thorax	M_3 : 24.9 Kg	L_3 : 1.308 m
4	Abdomen	M_4 : 2.4 Kg	L_4 : 1.099 m
5	Pelvis	M_5 : 11.8 Kg	L_5 : 0.983 m
6	Arms	M_6 : 4 Kg	L_6 : 1.285 m
7	Forearms	M_7 : 2.8 Kg	L_7 : 1.027 m
8	Hands	M_8 : 1 Kg	L_8 : 0.792 m
9	Thighs	M_9 : 19.6 Kg	L_9 : 0.75 m
10	Calfs	M_{10} : 7.6 Kg	L_{10} : 0.33 m
11	Feet	M_{11} : 2 Kg	L_{11} : 0.028 m
12	Hip Pivot to Ground		L_{12} : 0.946 m
13	Knee Pivot to Ground		L_{13} : 0.505 m

B. Posture Detection and Low-Level Torque Control

In our biomechanics model based control strategy, it automatically assists the wearer for both squat and stoops. [13] used a predefined and fixed torque reference and it only worked with a stoop or squat motion instead of the adaptive and generic reference torque in our method. The high-level controller runs at 1K Hz and the torque loop proportional-integral-derivative (PID) controller is implemented to track the reference assistive torque. The low-level controller is implemented by the velocity loop PID which runs at 20K Hz, and the current PID control runs at 200K Hz. The sample rate of the IMUs is 400 Hz. The three x-axes Euler angles of IMUs are represented as trunk angle θ_b , thigh angle θ_t , and shank angle θ_s and they are calibrated to zero degrees at the beginning of the experiment when the subject was instructed to stand straight. The knee angle θ_k and hip angle θ_h are calculated by equation (8)-(9) and the positive direct of knee and hip is an extension.

$$\theta_k = \theta_t - \theta_s \quad (8)$$

$$\theta_h = \theta_t - \theta_b \quad (9)$$

C. Experimental Procedure and Squat Assistant Control

To evaluate the assistive control, the experiments include five tests, namely squatting without exoskeleton, zero torque tracking control, 10%, 30%, and 50% of biological torque assistance, were performed by a 26-year healthy male without any movement disorders. The study was approved by the City University of New York Institutional Review Board, and all methods were carried out in accordance with the approved study protocol.

The subject followed a metronome to perform the 8 second squat shown as Fig. 9 and repeat 5 times for each experiment. The knee angle θ_k , desired assistive torque τ_r , actual assistive torque, raw EMG signal and average of root-mean-square (RMS) EMG signal was used to analyze the resistance during squat in the unpowered condition and zero torque control. The torque control tracking error was also analyzed in the experiments with 10% assistance, 30% assistance, 50 % assistance. Because the main contributed muscle is knee extensor in the squat, the assistive effect was evaluated by comparing the average of RMS EMG from knee extensor (Rectus Femoris) between the 5 conditions (without exoskeleton, zero torque control, 10% assistance, 30%

assistance, 50% assistance). The average of RMS EMG was calculated by rectifying the raw EMG, RMS calculation with 0.3 s window, and average the RMS EMG in 5 squat cycles.

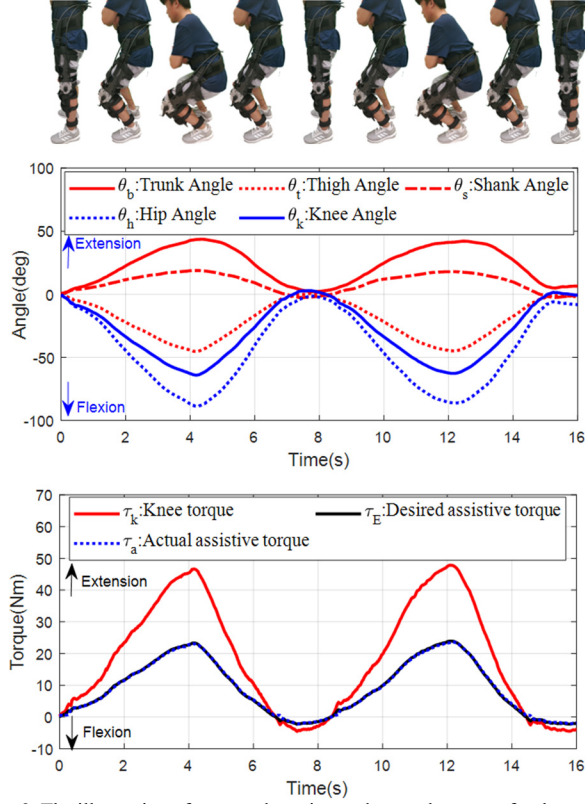


Fig. 9. The illustration of gesture detection and control strategy for the squat experiment with 50% of biological torque assistance. The top graph demonstrates the trunk, hip, thigh, knee, and shank angles with respect to time during the squat movement. The bottom graph depicts the biological knee, desired assistive, and actual assistive torques as a function of time.

VI. EXPERIMENTAL RESULTS

To demonstrate the high-backdrivability characteristics, the control performance, and assistive performance, the results of the experiment of resistive torque in unpowered condition, the resistive torque in zero torque tracking control, the tracking performance in assistive control, and the evaluation of assistive control are described in this section.

A. High-Backdrivability in Unpowered Condition

For the demonstration of the high-backdrivability, the resistive torque during squat in unpowered condition was studied. Thanks to quasi direct drive actuation and cable-drive mechanism, it generates low impedance as the maximum resistive torque is 2.58 Nm which took place in the onsets of motor rotation and the changes of the direction. The average of the absolute resistance is 0.92 Nm, as shown in Fig. 10. Subjects reported extremely low resistance when wearing the device.

B. Zero Torque Tracking Control

The subject performed squatting to investigate the characteristics of resistive torque during the zero torque

tracking control. Its reference torque is set to zero regardless of human motion. The zero torque control is implemented to eliminate the mechanical resistance, such as friction of the cables and gears. In the Fig. 11, the blue line indicates the measured torque and the orange line indicates the knee angle. The maximum measured torque (mechanical resistance) is approximate to 0.64 Nm and the average of absolute measured torque is 0.34 Nm. Comparing to the unpowered condition, the maximum torque in zero torque control is further reduced by 4 times and the average of the absolute measured torque in zero torque control is reduced 2.7 times. Therefore, it guarantees that the exoskeleton does not increase the human energy consumption due to the mechanical resistance using the zero torque tracking control.

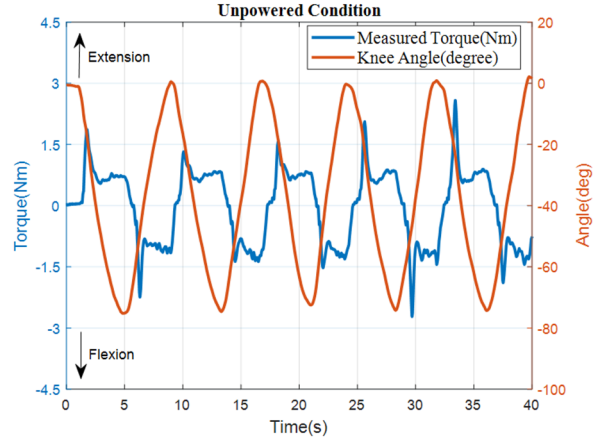


Fig. 10. The result of the resistive torque characterization during squatting. The maximum torque of the mechanical resistance is 2.58 Nm and the average torque is 0.92 Nm. It reveals that our robot is highly backdrivable with low resistance.

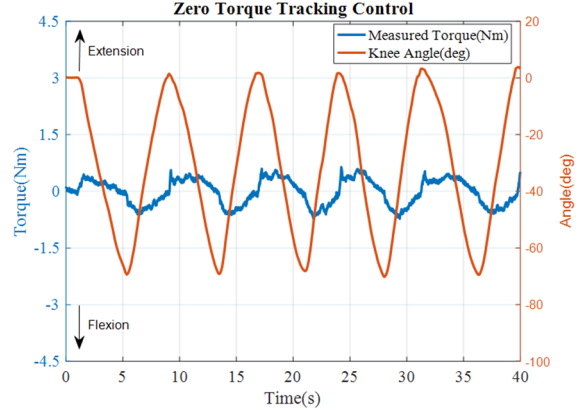


Fig. 11. The result of the zero torque tracking control. The reference torque is set to zero. It demonstrates that the maximum resistive torque is approximately 0.64 Nm and the average of the absolute measured torque is 0.34 Nm. It reveals that the zero torque tracking control further reduces the mechanical resistance on top of the intrinsic low impedance due to quasi direct drive actuation.

C. Torque Tracking for Squatting Assistance

Tests for 10%, 30%, and 50% of biological knee joint torque assistance were performed to investigate the tracking performance. The knee torque τ_k were calculated by equation (1) and the desired assistive torque τ_r is calculated by equation (2). The gain is set at 0.1, 0.3, and 0.5 in the 10%, 30%, and 50% assistive control respectively. The assistive control was used to assist human knee joint by applying specific torque

according the current trunk angle θ_b and thigh angle θ_t during the squat cycle. The angles of human segments were detected by the IMU sensors mounted on the trunk, thigh, and shank. The tracking perform is shown in Fig. 12. The RMS of the absolute error between the desired and actual torque trajectory was 0.23 Nm (2.8% of 7.6 Nm torque peak) in 10% knee assistance, 0.22 Nm (1.1% of 20 Nm peak torque) in 30% knee assistance, and 0.29 Nm (1.2% of 23.9 Nm peak torque) for 50% knee assistance. It demonstrated that the torque controller can follow accurately and reliably deliver the desired the torque profile to assist squatting.

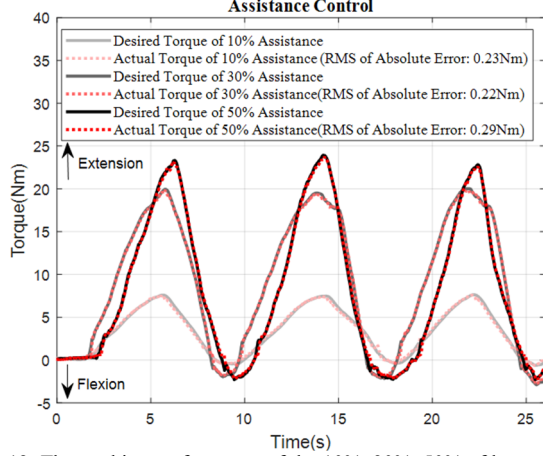


Fig. 12. The tracking performance of the 10%, 30%, 50% of knee torque assistance in three squatting cycles. The RMS of the absolute error between the desired and actual torque trajectory is 0.3 Nm, 0.22 Nm, and 0.29 Nm in 10%, 30%, and 50% knee assistance.

D. Injury Prevention Demonstration with EMG Sensors

The effectiveness of muscle activity reduction using the assistive control was evaluated in 5 condition. As shown in Fig. 13, the average of RMS EMG in 5 squat cycles were calculated and used to compare the amplitude in different conditions (without wearing the exoskeleton, zero torque control, 10%, 30%, and 50% assistance). It depicts that the more torque delivered to the subject, the more muscle activities were reduced. The EMG has similar amplitude in the conditions of without exoskeleton, zero torque control, and 10% assistance. But the squat with 10% assistance has the highest amplitude. It indicates that 1) the exoskeleton does not restrict natural movement as EMG had similar amplitude in without exoskeleton and zero torque control; 2) the assistance percentage should be large enough to reduce the muscle effort and the squat with 30% and 50% assistance can reduce the muscle effort effectively. Comparing to the squat without exoskeleton, the maximum amplitude of knee extensor muscle activity (rectus femoris) measured by EMG sensors was reduced by 30% using 50 % assistance.

The Fig. 14 shows the raw EMG signal and knee angle during squat without exoskeleton and with 50% assistance. It shows that the amplitude of the raw EMG signal in squatting with 50% assistance is smaller and it also reveals that the assistive control could reduce the muscle effort of knee extensor.

VII. DISCUSSION AND CONCLUSION

This paper presents our endeavor to develop comfort-centered high performance exoskeletons that minimize discomfort, reduce weight, and enhance symbiotic control between human and robots. Discomfort minimization is treated as an engineering solution to mitigate high pressure concentration (our hybrid exoskeleton design maximizes moment arm) and reduce impedance (quasi-direct drive actuation ensures high backdrivability). Weight minimization is achieved with high torque density motor and bidirectional cable drive using a single motor. As proof of concept, the tethered exoskeleton demonstrates the design principles and effectiveness of control strategies. All design principles are transferable to portable version. Moreover, the offboard actuator is also lightweight. Our future work will investigate optimal control strategies using this platform and study the effectiveness of a portable version in the field using wearable motion and physiology sensors for injury prevention and human augmentation.

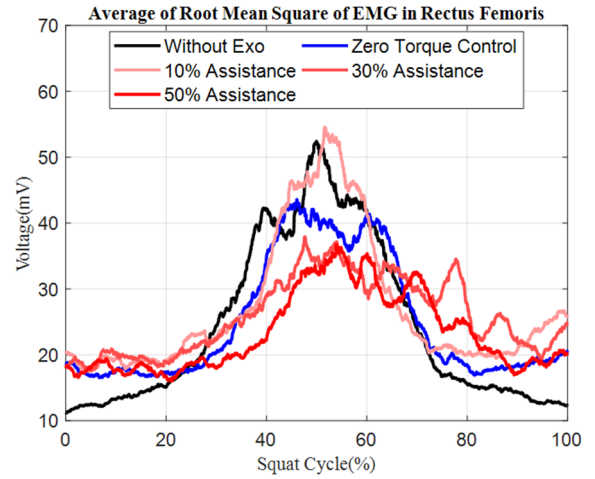


Fig. 13. The result of the assistive control. It shows the average of RMS EMG in 5 squat cycles. The x-axis is the squat cycle and the y-axis is the average of RMS EMG. There are 5 conditions (without Exo, zero torque control, 10% assistance, 30% assistance, 50% assistance) compared. It reveals the higher percentage of assistance has the tendency to reduce the amplitude of the RMS EMG.

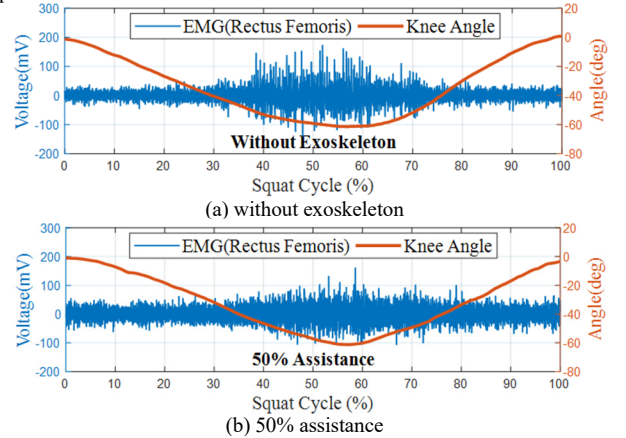


Fig. 14. Comparing the result between the squat without exoskeleton and squat with 50% assistance. It shows the amplitude of raw EMG signal in squat with 50% assistance is smaller and it reveal the assistive control could help to reduce the muscle effort in knee extensor.

REFERENCES

- [1] Liberty Mutual Insurance Company, Safety Index, 2017
- [2] M. P. de Looze, T. Bosch, F. Krause, K. S. Stadler, and L. W. O'Sullivan, "Exoskeletons for industrial application and their potential effects on physical work load," (in English), *Ergonomics*, vol. 59, no. 5, pp. 671-681, May 2016.
- [3] Y. Ding, M. Kim, S. Kuindersma, and C. J. Walsh, "Human-in-the-loop optimization of hip assistance with a soft exosuit during walking," *Science Robotics*, vol. 3, no. 15, p. eaar5438, 2018.
- [4] J. Zhang, P. Fiers, K. A. Witte, R. W. Jackson, K. L. Poggensee, C. G. Atkeson, and S. H. Collins, "Human-in-the-loop optimization of exoskeleton assistance during walking," *Science*, vol. 356, no. 6344, pp. 1280-1284, Jun 23 2017.
- [5] S. H. Collins, M. B. Wiggins, and G. S. Sawicki, "Reducing the energy cost of human walking using an unpowered exoskeleton," *Nature*, vol. 522, no. 7555, p. 212, 2015.
- [6] Z. F. Lerner, D. L. Damiano, and T. C. Bulea, "A lower-extremity exoskeleton improves knee extension in children with crouch gait from cerebral palsy," *Science translational medicine*, vol. 9, no. 404, p. eaam9145, 2017.
- [7] X. Jin, A. Prado, and S. K. Agrawal, "Retraining of Human Gait-Are Lightweight Cable-Driven Leg Exoskeleton Designs Effective?," *IEEE Transactions on Neural Systems and Rehabilitation Engineering*, vol. 26, no. 4, pp. 847-855, 2018.
- [8] N. Vitiello, S. Mohammed, and J. C. Moreno, "Wearable robotics for motion assistance and rehabilitation," *Robotics and Autonomous Systems*, vol. 73, no. C, pp. 1-3, 2015.
- [9] J. F. Veneman, R. Kruidhof, E. E. Hekman, R. Ekkelenkamp, E. H. Van Asseldonk, and H. Van Der Kooij, "Design and evaluation of the LOPES exoskeleton robot for interactive gait rehabilitation," *IEEE Transactions on Neural Systems and Rehabilitation Engineering*, vol. 15, no. 3, pp. 379-386, 2007.
- [10] M. B. Näf, A. S. Koopman, S. Baltrusch, C. Rodriguez-Guerrero, B. Vanderborght, and D. Lefeber, "Passive Back Support Exoskeleton Improves Range of Motion Using Flexible Beams," *Frontiers in Robotics and AI*, vol. 5, 2018.
- [11] K. Shang, X. Xu, and H. Su, "Design and evaluation of an upper extremity wearable robot with payload balancing for human augmentation," in *2017 International Symposium on Wearable Robotics and Rehabilitation (WeRob)*, 2017, pp. 1-1: IEEE.
- [12] S. Toxiri, A. S. Koopman, M. Lazzaroni, J. Ortiz, V. Power, M. P. de Looze, L. O'Sullivan, and D. G. Caldwell, "Rationale, Implementation and Evaluation of Assistive Strategies for an Active Back-Support Exoskeleton," *Frontiers in Robotics and AI*, vol. 5, 2018.
- [13] B. Chen, L. Grazi, F. Lanotte, N. Vitiello, and S. Crea, "A Real-Time Lift Detection Strategy for a Hip Exoskeleton," *Frontiers in neurorobotics*, vol. 12, p. 17, 2018.
- [14] C. R. Reid, P. M. Bush, N. H. Cummings, D. L. McMullin, and S. K. Durrani, "A review of occupational knee disorders," *Journal of occupational rehabilitation*, vol. 20, no. 4, pp. 489-501, 2010.
- [15] T. Bacek, M. Molledo, C. Rodriguez-Guerrero, J. Geeroms, B. Vanderborght, and D. Lefeber, "Design and evaluation of a torque-controllable knee joint actuator with adjustable series compliance and parallel elasticity," *Mechanism and Machine Theory*, vol. 130, pp. 71-85, 2018.
- [16] N. Karavas, A. Ajoudani, N. Tsagarakis, J. Saglia, A. Bicchi, and D. Caldwell, "Tele-impedance based stiffness and motion augmentation for a knee exoskeleton device," in *Robotics and Automation (ICRA), 2013 IEEE International Conference on*, 2013, pp. 2194-2200: IEEE.
- [17] J. E. Pratt, B. T. Krupp, C. J. Morse, and S. H. Collins, "The RoboKnee: an exoskeleton for enhancing strength and endurance during walking," in *Robotics and Automation, 2004. Proceedings. ICRA'04. 2004 IEEE International Conference on*, 2004, vol. 3, pp. 2430-2435: IEEE.
- [18] K. A. Witte, A. M. Fatschel, and S. H. Collins, "Design of a lightweight, tethered, torque-controlled knee exoskeleton," in *Rehabilitation Robotics (ICORR), 2017 International Conference on*, 2017, pp. 1646-1653: IEEE.
- [19] G. Elliott, A. Marecki, and H. Herr, "Design of a clutch-spring knee exoskeleton for running," *Journal of Medical Devices*, vol. 8, no. 3, p. 031002, 2014.
- [20] K. Shamaei, M. Cenciari, A. A. Adams, K. N. Gregorczyk, J. M. Schiffman, and A. M. Dollar, "Design and Evaluation of a Quasi-Passive Knee Exoskeleton for Investigation of Motor Adaptation in Lower Extremity Joints," (in English), *Ieee Transactions on Biomedical Engineering*, vol. 61, no. 6, pp. 1809-1821, Jun 2014.
- [21] M. K. Shepherd and E. J. Rouse, "Design and Validation of a Torque-Controllable Knee Exoskeleton for Sit-to-Stand Assistance," *IEEE/ASME Transactions on Mechatronics*, vol. 22, no. 4, pp. 1695-1704, 2017.
- [22] J. C. McLeod, S. J. Ward, and A. L. Hicks, "Evaluation of the Keeogo Dermoskeleton," *Disabil Rehabil Assist Technol*, pp. 1-10, Nov 2 2017.
- [23] S. Sridar, P. H. Nguyen, M. Zhu, Q. P. Lam, and P. Polygerinos, "Development of a soft-inflatable exosuit for knee rehabilitation," in *Intelligent Robots and Systems (IROS), 2017 IEEE/RSJ International Conference on*, 2017, pp. 3722-3727: IEEE.
- [24] J. S. Sulzer, R. A. Roiz, M. A. Peshkin, and J. L. Patton, "A Highly Backdrivable, Lightweight Knee Actuator for Investigating Gait in Stroke," *IEEE Trans Robot*, vol. 25, no. 3, pp. 539-548, Jun 2009.
- [25] J. Wolff, C. Parker, J. Borisoff, W. B. Mortenson, and J. Mattie, "A survey of stakeholder perspectives on exoskeleton technology," *Journal of neuroengineering and rehabilitation*, vol. 11, no. 1, p. 169, 2014.
- [26] D. Park and K.-J. Cho, "Development and evaluation of a soft wearable weight support device for reducing muscle fatigue on shoulder," *PloS one*, vol. 12, no. 3, p. e0173730, 2017.
- [27] V. Bartenbach, M. Gort, and R. Riener, "Concept and design of a modular lower limb exoskeleton," in *Biomedical Robotics and Biomechanics (BioRob), 2016 6th IEEE International Conference on*, 2016, pp. 649-654: IEEE.
- [28] P. M. Wensing, A. Wang, S. Seok, D. Otten, J. Lang, and S. Kim, "Proprioceptive actuator design in the MIT cheetah: Impact mitigation and high-bandwidth physical interaction for dynamic legged robots," *IEEE Transactions on Robotics*, vol. 33, no. 3, pp. 509-522, 2017.
- [29] Y. Ding and H.-W. Park, "Design and experimental implementation of a quasi-direct-drive leg for optimized jumping," 2017.
- [30] S. Yu, Y. Li, T.-H. Huang, J. Wang, X. Li, and H. Su, "A Quasi-Direct-Drive Cable Actuation System for An Intrinsically Safe Knee Exoskeleton," *Dynamic Walking*, 2018.
- [31] J. Wang, X. Li, T.-H. Huang, S. Yu, Y. Li, T. Chen, A. Carriero, M. Oh-Park, and H. Su, "Comfort-Centered Design of a Lightweight and Backdrivable Knee Exoskeleton," *IEEE Robotics and Automation Letters*, 2018.
- [32] K. Schmidt, J. E. Duarte, M. Grimmer, A. Sancho-Puchades, H. Wei, C. S. Easthope, and R. Riener, "The myosuit: Bi-articular anti-gravity exosuit that reduces hip extensor activity in sitting transfers," *Frontiers in neurorobotics*, vol. 11, p. 57, 2017.
- [33] A. Gams, T. Petric, T. Debevec, and J. Babic, "Effects of robotic knee exoskeleton on human energy expenditure," *IEEE Trans Biomed Eng*, vol. 60, no. 6, pp. 1636-44, Jun 2013.
- [34] H. G. Armstrong, "Anthropometry and mass distribution for human analogues," *Military male aviators*, vol. 1, 1988.